



# Electrochemical reforming of glycerol into hydrogen in a batch-stirred electrochemical tank reactor equipped with stainless steel electrodes: Parametric optimization, total operating cost, and life cycle assessment

Ever Peralta-Reyes<sup>a</sup>, Diego Vizarratea-Vásquez<sup>a</sup>, Reyna Natividad<sup>b</sup>, Aitor Aizpuru<sup>a</sup>, Edson Robles-Gómez<sup>a</sup>, Claudia Alanis<sup>b</sup>, Alejandro Regalado-Méndez<sup>a,\*</sup>

<sup>a</sup> Investigation Laboratories, Campus Puerto Ángel, Universidad del Mar, Puerto Ángel 70902, Oaxaca, Mexico

<sup>b</sup> Chemical Engineering Laboratory, Centro Conjunto de Investigación en Química Sustentable, UAEMex-UNAM, Universidad Autónoma del Estado de México, Toluca 50200, Estado de México, Mexico

## ARTICLE INFO

Editor: Despo Kassinos

### Keywords:

Biodiesel  
Electrochemical reforming  
Hydrogen  
Life cycle assessment  
Parametric optimization  
Waste glycerol

## ABSTRACT

The electrochemical reforming of glycerol was carried out in a batch-stirred electrochemical tank reactor equipped with stainless steel electrodes. A response surface methodology constituted by a Face-Centered Central Composite Design was performed to establish the optimal operational conditions to produce hydrogen. Studied parameters were glycerol concentration ( $C_G$ ), current intensity ( $I$ ) and temperature ( $T$ ), while chosen responses were hydrogen and oxygen concentrations ( $C_{H_2}$  and  $C_{O_2}$ ). A maximum  $C_{H_2}$  (79.18 mg/L) and minimum  $C_{O_2}$  (46.24 mg/L) with a global desirability of 67%, were achieved at multi-optimal conditions, including  $C_G = 3.46$  mol/L,  $I = 5.21$  A, and  $T = 70$  °C. All studied parameters were significant for both chosen responses ( $\eta_{C_{H_2}}$  and  $\eta_{C_{O_2}}$ ) since all values of the sensitivity index were higher than 0.5. The analysis of interaction between parameters suggests that  $C_G$  and  $T$  simultaneous increase will bring a decrease in  $C_{H_2}$ . The experimental data were fitted to a quadratic polynomial surrogate model, with correlation coefficients of 0.9801 and 0.9967 for  $\eta_{C_{H_2}}$  and  $\eta_{C_{O_2}}$ , respectively. The reduced root-mean-square error was 0.065 and 0.054 for  $\eta_{C_{H_2}}$  and  $\eta_{C_{O_2}}$ , respectively. This suggests a successful optimization of the BSETR operational parameters. The hydrogen production process assessed in this work, is a promising green energy technology that uses waste glycerol as a carbon-based fuel and a low-cost anode material (7.5 USD€/kg H<sub>2</sub>) as stainless steel. The carbon footprint of the hydrogen production by the optimized process is 0.192 kg CO<sub>2</sub> eq and this can be reduced 92.1% when using a solar photovoltaic system to energize the electrodes.

## 1. Introduction

Current worldwide contamination is mainly caused by the excessive use of fossil fuels, which reduces air quality, affects human health, and raises global warming. Under this framework, scientific efforts are focused on the production of novel renewable fuels such as bioethanol [1], biodiesel [2], and hydrogen [3]. Hydrogen (H<sub>2</sub>) was declared as a zero-emissions fuel [4]. Also, H<sub>2</sub> is an effective, green, and renewable energy source [5] (with a high heating value of 142 kJ/g [6]), which can be obtained from the disintegration of organic molecules through different methods [7] such as steam reforming [8], thermal reforming

[9], electrochemical reforming [10], and others [11–13]. The electrochemical reforming of carbon-based fuels (e.g. low rank coal, biomass, commercial carbon, alcohols, and natural gas) can be conducted in an electrolytic cell at low temperature and atmospheric pressure [14]. One of the advantages of this last method is the production of high-purity hydrogen at the cathode, eliminating the need of further separation and purification [15]. In this context, glycerol has been suggested as a cost-effective compound to produce hydrogen [16], leading to a sustainable hydrogen production process [17], and also to added-value chemicals [18,19] such as tartronic acid, glyceraldehyde, mesoxalic acid, glyceric acid, dihydroxyacetone, lactic acid, formic acid, 1, 3-propanediol, formaldehyde, and 1, 2-propanediol [20,21], and others [22].

\* Corresponding author.

E-mail addresses: [pere@angel.umar.mx](mailto:pere@angel.umar.mx) (E. Peralta-Reyes), [diegovizarratea@gmail.com](mailto:diegovizarratea@gmail.com) (D. Vizarratea-Vásquez), [reynanr@gmail.com](mailto:reynanr@gmail.com) (R. Natividad), [aitor@angel.umar.mx](mailto:aitor@angel.umar.mx) (A. Aizpuru), [edson@angel.umar.mx](mailto:edson@angel.umar.mx) (E. Robles-Gómez), [claudia.alanis.iq@gmail.com](mailto:claudia.alanis.iq@gmail.com) (C. Alanis), [alejandro.regalado33@gmail.com](mailto:alejandro.regalado33@gmail.com), [regalado@angel.umar.mx](mailto:regalado@angel.umar.mx) (A. Regalado-Méndez).

<https://doi.org/10.1016/j.jece.2022.108108>

Received 30 October 2021; Received in revised form 31 May 2022; Accepted 15 June 2022

Available online 17 June 2022

2213-3437/© 2022 Elsevier Ltd. All rights reserved.

**Nomenclature**

## Symbols Meaning.

AR	Total surface area (m <sup>2</sup> ).
C	Concentration (mg/L).
c	Cost (USD).
E	Energy (kWh/L).
F	Faraday constant (96,485 C/mol).
H <sub>2</sub>	Hydrogen.
I	Current intensity (A).
M	Molecular mass of iron (g/mol).
Mass	Mass generated (kg).
n	Number of experiments.
N <sub>2</sub>	Nitrogen.
O <sub>2</sub>	Oxygen.
q	Quantity of external chemical used (kg).
R <sub>2</sub>	Correlation coefficient.
T	Temperature (°C).
t	Time (h).
TotalOC	Total operational cost (USD\$/kg).
TOC	Total organic carbon (mg).
U	Average potential (V).
x	Uncoded independent variables.
X	Coded independent variables (dimensionless).
z	Number of electrons transferred (z = 2).

**Acronyms**

ANOVA	Analysis of variance.
AE	Alkaline electrolyzer.
AME	alkaline membrane electrolyzer.
AEME	Alkaline exchange membrane electrolyzer.
BSETR	Batch-stirred electrochemical tank reactor.
CCD	Central composite design.
DAFC	Direct alkaline fuel cell.
FCCCD	Face-Centered Central Composite design.
F-value	Is a value on the F distribution.

LCA	Life cycle assessment.
LCI	Life cycle inventory.
PEM	Polymer Electrolyte Membrane.
p-value	Is a measure of the probability that an observed difference could have occurred just by random chance.
RSM	Response surface methodology.
RMSE	Reduced root-mean-square error.
S	Sensitivity index.
SS	Stainless-steel.

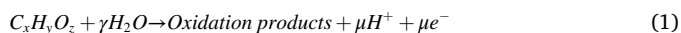
**Greek letters**

α	Electricity price (USD/kWh).
β	Coefficients of the quadratic model.
γ	Stoichiometric coefficients of reaction at cathode electrode.
Δ	Increment.
ε	Random error.
ξ	Electrode material price (USD/Kg stainless steel).
φ	Price of electrolyte (USD/kg).
η	Response.
μ	Stoichiometric coefficient.
ρ	Density (g/cm <sup>3</sup> ).

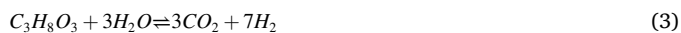
**Subscripts**

Ac	Active anode.
Adj	Adjusted.
cell	Electrochemical cell.
con	Consumption.
Exp	Experimental.
G	Glycerol.
i	Variable number.
j	Variable number different to i.
k	Response; $\eta_{C_{H_2}}$ and $\eta_{C_{O_2}}$ .
Pred	Predicted.
rxn	Reaction.

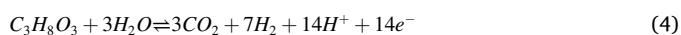
In addition, glycerol is the principal by-product of biodiesel production processes [23] and is often unused because of its high impurity, difficulty and high-cost purification. Therefore, its consumption and disposal are becoming important issues from an environmental point of view. In this sense, one promising process to transform glycerol is electrochemical reforming. This process consists in the organic compound electro-oxidation at the anode, which generates protons and products of the organic oxidation (see Eq. (1)), hydrogen is then concomitantly produced at the cathode by means of reaction (2) [24,25],



In this sense, the electrochemical reforming of glycerol can be described by Eq. (3), assuming that glycerol is oxidized completely into carbon dioxide with the addition of water,



Eqs. (4) and (5) represent the anode and cathode reactions, respectively:



Since reactions (4) and (5) proceed at the anode and cathode, respectively; the electrodes material is important since it dictates the

efficiency of the process. There are summarized in Table 1, the different electrode materials that have been assessed to produce hydrogen from glycerol electrochemical reforming. It can be observed that the existing literature is dominated by Pt, Pd and Au based electrocatalysts. Regarding Pt, this has been combined with other metals like Ru and Ir and has been supported on Nafion 117 membrane; which led to save 66% of electrical energy compared to electrolysis. Despite this improvement, the used electrocatalyst was slowly poisoned by glycerol and/or by its oxidation products [16]. There also have been interesting works with Pd, like that conducted in a 3D-Printed cell equipped with Pd nanocubes supported on a glassy carbon as working electrode and Nafion 424 membrane [26]; although an important extent of selectivity (99%) towards tartronate production was obtained, a low hydrogen production was observed. Also, the glycerol electrochemical reforming has been performed in an alkaline exchange membrane electrolyzer (AEME) with a Pd/TNTA anode electrode [27], where an excellent activity and high output current densities were observed, and thus the energy balance was advantageous over PEM water electrolysis. Despite saving energy for hydrogen production, in such a work, the major process cost is assumed by the NaOH use. In other work, the direct alkaline fuel cell (DAFC) [29] was coupled with Pd-(Ni-Zn)/C on foam anode as a strategy to increase the selectivity of hydrogen production; nevertheless, carbonate was produced by the oxidation products, which could result in the loss of the available electro-active surface area by the electrocatalyst poisoning [26,31]. In other works, the alkaline membrane electrolyzer (AME) was employed in the glycerol electrochemical

**Table 1**  
Literature review of glycerol electrochemical reforming.

Electrochemical cell	Electrolyte/ Membrane	Anode	Cathode	Ref.
Three-electrode glass	H <sub>2</sub> SO <sub>4</sub> /—	Pt/C	Pt	[34]
AME	KOH/+	Pt/C	Pt/C	[32]
AME	—/+	PtRu/C	Pt/C	[33]
PEME	H <sub>2</sub> SO <sub>4</sub> / Nafion 117	Pt@RuIr oxide	Pt	[16]
Glass cell with coaxial electrodes	H <sub>2</sub> SO <sub>4</sub> /—	Pt grid	Pt grid	[36]
3D-Printed Electrolyzer	KOH/Nafion 424	Pd nanocubes	Pt	[26]
AEME	NaOH/ TAEM A201	Pd on TiO <sub>2</sub> nanotubes	Pt/C	[27]
DAFC	KOH/—	Pd-(Ni-Zn)/C on foam	—	[30]
AEME	KOH/TAEM A006	Pd-(Ni-Zn)/C on foam	Au	[28]
Three-electrode glass	NaOH/—	Pt/C, Au/C, Pd/C, Pd <sub>x</sub> Au <sub>y</sub> /C, Pd <sub>x</sub> Ni <sub>y</sub> , Pd <sub>x</sub> Bi <sub>y</sub> /C, Pt <sub>0.9</sub> Bi <sub>0.1</sub> and Pd <sub>0.45</sub> Pt <sub>0.45</sub> Bi <sub>0.1</sub>	—	[35]
AE	NaOH/ Absorbent paper	Pt/C, Pt <sub>9</sub> Bi <sub>1</sub> /C or Pt <sub>3</sub> Pd <sub>6</sub> Bi <sub>1</sub> /C	Pt	[37]
AME	—/+	Pt/C, Pt <sub>3</sub> Bi/C, PtBi/C, Pd/C, Pd <sub>3</sub> Bi/C, Au/C and Au <sub>3</sub> Ag/C	Pt/C	[31]
Pyrex glass	KOH/—	Ti/RuO <sub>2</sub> , Pt grid	SS	[18]

DAFC: Direct alkaline fuel cell; AE: alkaline electrolyzer; AME: alkaline membrane electrolyzer; PEME: proton exchange membrane electrolyzer; AEME: Alkaline exchange membrane electrolyzer; + : KOH-doped Polybenzimidazole (PBI); TAEM: Tokuyama anion-exchange membrane.

reforming by coupling different electrocatalysts (e.g., (Pt/C, Pt<sub>3</sub>Bi/C, PtBi/C, Au/C, Au<sub>3</sub>Ag/C, Pd/C and Pd<sub>3</sub>Bi/C) [31,32]), these alters the selectivity to C<sub>3</sub> carboxylates but the carbon mass balance is positive and this may be associated once again with formation of carbonates. Although the energy consumption of AME is lower than that of KOH-doped Polybenzimidazole (PBI) water cells, the hydrogen production rate must be improved [33]. Three-electrode glass cell is another type of cell that has been employed to produce hydrogen using glycerol as fuel stock in acid media [34] using a Pt/C as work electrode and alkali media [35] using an electrocatalyst based on Pd, Au, Ni, Pt, Bi, and Ag in different proportions, prepared by an emulsion method. Although the hydrogen production and selectivity to produce C<sub>3</sub> carboxylates compounds was improved, authors comment that such a type of electrocatalyst is expensive and thus the electrolysis cell is suggested to be designed with Pt-free electrocatalysts. Other approach to conduct the glycerol electrochemical reforming is in a glass cell with coaxial electrodes (Pt grid in a cylindrical shape) under strong acid media and low current density to produce hydrogen and valuable compound (e.g., formic acid, glycidol, propanediol, 2-propenol, and amongst others). The room for improvement of this process is to use an electrocatalyst able to provide a high selectivity and yield of valuable compounds, with less Pt [36]. Additionally, the hydrogen was produced in an alkaline electrolyzer (AE) coupled with an electrocatalyst based on Pt, Pd, and Bi such as Pt/C, Pt<sub>9</sub>Bi<sub>1</sub>/C, and Pt<sub>3</sub>Pd<sub>6</sub>Bi<sub>1</sub>/C [37]. Although it was demonstrated that this strategy leads to saving a 60% of electrical energy compared with a commercial water electrolysis cell and that the developed electrocatalyst has an 80% of selectivity towards glycerol-dehyde, the glycerol conversion was only about 6%. In summary, the search remains for electrocatalysts to produce hydrogen from glycerol with lower energy consumption than electrolysis cells and with lower cost than those Pt or Pd-based, which in turn will improve the economic viability of the reforming process at large scale. In this connection, to make the electrochemical reforming process cost-effective, the stainless-steel (SS) electrodes could be useful since is one type of

electrode that is often used in the water treatment through electrolysis because of similar anodic properties and electrochemical corrosion resistance than electrocatalysts based on expensive metals [38]. In addition, it can also be concluded from the literature review, that the studies reported in Table 1, overlook the optimization of the process and the implied environmental impacts. These are directly related to the process sustainability and therefore are important in the visualization of a decarbonized future scenario. In this regard, the quantification of relevant emissions and consumed resources is advised. For this purpose, a life cycle assessment (LCA) can be conducted since is a structured and international standardized method that allows the evaluation of inputs, outputs, and potential environmental impacts of a process and thus LCA is widely accepted to evaluate the sustainability of processes and technologies to produce green chemicals.

Because of the above said, the objective of this work was to optimize the electrochemical reforming of commercial and crude glycerol carried out in a BSETR equipped with stainless steel electrodes. This was achieved by applying the response surface methodology (RSM) constituted by a Face-Centered Central Composite Design (FCCCD). The studied parameters were glycerol concentration ( $C_G$ ), current intensity ( $I$ ) and temperature ( $T$ ), while chosen responses were hydrogen and oxygen concentrations ( $\eta_{\text{CH}_2}$  and  $\eta_{\text{CO}_2}$ , respectively). In addition, the carbon footprint of the optimized process was estimated by LCA. A contribution analysis to the midpoint impact categories was also performed. Finally, the effect of the source of energy for the electrodes on the carbon footprint and on the endpoint impact categories, was established by comparing two scenarios, fossil fuels and solar photovoltaics energy.

## 2. Materials and methods

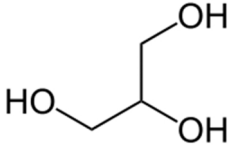
### 2.1. Preparation of synthetic aqueous glycerol solution

All experiments were conducted with 0.5 L of aqueous solution containing commercial glycerol at different glycerol concentrations ( $C_G$ ) according to Table S1 and Na<sub>2</sub>SO<sub>4</sub>, 0.5 M as supporting electrolyte. This aqueous solution was prepared by adding the reagents into a BSETR with distilled water until a homogeneous mixture was obtained. The commercial glycerol (99.7% purity) was purchased from La Corona Company (Ecatepec, Edo. Mex., Mexico) and the Na<sub>2</sub>SO<sub>4</sub> (99% purity) was supplied by Karal Group (León, Gto., Mexico). The chemical formula and some physicochemical properties of glycerol are shown in Table 2.

### 2.2. Experimental set-up

The experimental set-up is constituted by a BSETR (see Fig. S1) with a total volume of 640 cm<sup>3</sup>, two stainless steel electrodes (grade 304 with a thickness of 1.22 mm) with a total surface area of 83.22 cm<sup>2</sup> ( $AR_{Ac}$ ) that are separated 2 cm from each other. Before each experiment, the electrodes were washed with a 0.5 M HCl solution to remove any possible residue formed during previous tests. A magnetic bar was employed to maintain the glycerol-water mixture homogenous (see Section 2.1), and to enhance the mass transfer in the reaction system. Also, a cooling jacket was installed to maintain constant the temperature

**Table 2**  
Physicochemical properties of glycerol [39].

CAS Numbers:	56–81-5	Molecular structure of glycerol
Property	Value	
Molar weight (g/mol)	92.09	
Melting point (°C)	17.9	
Boiling point (°C)	290.0	
Flash point (°C)	> 400.0	
Water solubility (%)	Immiscible	
pH	6.4	
$\rho$ (g/cm <sup>3</sup> ) at 25 °C	1.31	

inside the BSETR. The energy was supplied by a single output DC power supply. Gas was collected at top of the reactor with a Tedlar sampling bag. The cooling water was provided by a submersible pump installed into a cool water bath vessel.

### 2.3. Electrochemical reforming of glycerol

In a typical experiment, 0.5 L of aqueous glycerol solution were loaded in the BSETR (see Fig. S1), 44.92 cm<sup>2</sup> was the electrode surface area in contact with the aqueous solution, and the stirring speed was set at 400 rpm. This solution was prepared according to Section 2.1. The studied variables were glycerol concentration ( $C_G$ ), current intensity ( $I$ ) and temperature ( $T$ ), according to Table 2. All experiments were performed by duplicate. The reported concentrations are the average of the obtained results. The total amount of experiments for the optimization of the hydrogen production process is shown in Table S1. The low, medium, and high levels of each operating variable that appear in Table 3 and Table S1 are coded as -1, 0, and +1, respectively. The operating variables tested here can be coded by using Eq. (6),

$$X_i = \frac{x_i - x_{i,0}}{\Delta x_i} \quad (6)$$

In this work, the values of the current intensity ( $I$ ) were selected as the conventional range used in electrochemical processes [40]. The temperature ( $T$ ) range was chosen according to the high hydrogen efficiency production previously reported [41] at intermediate temperatures (60 °C). Also, the glycerol concentration ( $C_G$ ) tested in this study was similar to the  $C_G$  employed in reference [16,42].

The produced gas was captured in a Tedlar sampling bag with a total volume of 1 L. Samples were taken after 40–80 min of reactor start-up, to purge initial gas present in the reactor and represent the gaseous composition during the hydrogen process.

Once the optimal operating conditions were found, three additional experiments were performed with waste glycerol from different biodiesel production processes. The waste glycerol employed here was obtained in previous authors works by the methanolysis of recycled cooking oil employing different catalysts such as sea sand [43], coral waste [44], and KOH [45].

### 2.4. Chemical analyses

The gas produced in the BSETR was captured at top of the reactor with a Tedlar sampling bag and analyzed (hydrogen and oxygen, 0.1 mL) using an Agilent 6890 gas chromatograph equipped with a 30 m HP-PLOT Q capillary column and a thermal conductivity detector. Nitrogen (N<sub>2</sub>) was used as carrier gas at a rate of 3 mL/min. Injector, oven, and detector temperatures were set to 250, 40, and 250 °C, respectively. Also, the chromatograph was previously calibrated using H<sub>2</sub>, O<sub>2</sub> and CO<sub>2</sub> gas purchased in Infra Group.

For the UHPLC analysis, a liquid aliquot was taken from the BSETR at 80 min, filtered (nylon membrane 0.2 μm) to remove solid particles, and analyzed by Ultra high-performance liquid chromatography (UHPLC). The Vanquish ThermoScientific chromatograph equipped with a Refractive Index Detector (Thermo Scientific RefractoMax 521) was used to identify the glycerol and by-products of the electrochemical

**Table 3**  
Values and level of the independent variables.

Operating variables	Levels		
	-1	0	+1
$x_1$ : $C_G$ (mol/L)	2	3	4
$x_2$ : $I$ (A)	5	6	7
$x_3$ : $T$ (°C)	30	50	70

reforming of glycerol process. The column (5 μm, 7.8 × 300 mm, Carbomix Ca-NP) was kept at 80 °C with a flow rate of 0.6 mL/min (deionized water). For acid compounds, a column (9 μm, 7.8 × 300 mm, Aminex HPX-87 H) at 60 °C and a flow rate of 0.5 mL/min (3 mM H<sub>2</sub>SO<sub>4</sub> solution) was used. Also, the reaction products were quantified using calibration curves.

The Inorganic Carbon (IC) content was determined with a 6001 TOC analyzer (Shimadzu, Instrumentation and Service in Analytica, S.A. de C.V., Mexico). Before analysis, 100 μL of the previously filtered sample was added to a 10 mL volumetric flask with distilled water. The IC concentration was determined according to the corresponding calibration curve.

### 2.5. Optimization process

The response surface methodology (RSM) is a powerful method to assess the influence of process variables and to establish the optimum operating conditions with a relatively small quantity of experiments. To achieve the optimization of the electrochemical reforming of glycerol process, the glycerol concentration ( $C_G$ ), current intensity ( $I$ ) and temperature ( $T$ ) were optimized by RSM assuming a Face-Centered Central Composite Design (FCCCD, 2<sup>k-1</sup> factorial points, 2k axial points and k center points). The responses studied were the hydrogen concentration ( $\eta_{C_{H_2}}$ ) and the oxygen concentration ( $\eta_{C_{O_2}}$ ). The  $C_{H_2}$  must be maximized and the  $C_{O_2}$  must be minimized to reduce the explosiveness of the Hydrogen-Glycerol mixture. To determine the optimal operation conditions and their interaction during the hydrogen production by electrochemical reforming of glycerol, a quadratic model, Eq. (7), was employed.

$$\eta = \beta_0 + \sum_{i=1}^3 \beta_i X_i + \sum_{i=1}^3 \beta_{ii} X_i^2 + \sum_{j=1}^3 \sum_{i=1}^3 \beta_{ij} X_j X_i + \varepsilon \quad (7)$$

where  $\eta$  is the predicted response,  $\beta$  values are the regression coefficients,  $\varepsilon$  is the random error, and  $X_i$  and  $X_j$  are the dimensionless coded independent variables. The  $\beta$  values of the polynomial equation were computed by using step-wise regression such as recommended in [46]. An analysis of variance (ANOVA) was employed to evaluate the suitability of the second-degree polynomial function and the significance of the elements of the equation.

The assumption for the second-degree polynomial regression model includes: the behavior of a dependent variable ( $\eta$ ) can be explained by an additive relationship between the dependent variable and a set of  $i$  independent variables ( $x_i$ ,  $i = 1-3$ ), the relationship between the dependent variable and any independent variable is curvilinear, the independent variables ( $x_i$ ) are independent from each other, and the errors are independent, normally distributed with mean zero and a constant variance [47].

The experimental design, data analysis, and the plotting of experimental data and results were performed in the Design-Expert ® V. 10.0 software (Multion Consulting, Mexico City, Mexico). Finally, the model accuracy for the two responses was evaluated using the performance index of the reduced root-mean-square error (RMSE), which is represented by Eq. (8),

$$RMSE = \sqrt{\frac{1}{n} \sum_n \left( \frac{\eta_{k, \text{Pred}} - \eta_{k, \text{Exp}}}{\eta_{k, \text{Exp}}} \right)^2} \quad (8)$$

where  $\eta_{k, \text{Pred}}$  is the response obtained by the model,  $\eta_{k, \text{Exp}}$  is the response obtained experimentally, and  $n$  is the number of experiments.

### 2.6. Life cycle assessment (LCA)

The LCA follows the ISO 14044 standards [48,49]. A typical LCA implies the following stages: goal and scope definition, functional unit (FU), system description and boundaries, life cycle inventory (LCI),

impact assessment and interpretation. In this work, the goal was to evaluate the environmental impacts of the process to produce hydrogen by the electrochemical reforming of glycerol at optimum conditions and compare the results with those when a renewable source of energy, a solar photovoltaic system (PV), is used to energize the electrodes. The FU for this LCA was 1 MJ of hydrogen produced, all values refer to cradle to gate (see Fig. 1). Thus, the system boundary is depicted in Fig. 1 and this is useful to indicate the inputs and outputs to be considered in the LCI and the stages of the process to assess. According to Fig. 1, the LCA will focus on the stage of glycerol reforming and the LCI takes into account the reagents entering the system in the aqueous glycerol solution (glycerol, deionized water and sodium sulfate), another input is the electricity consumption and the recycled 304 stainless steel electrodes that can be used up to 17 times without the efficiency being affected. As indicated in Fig. 1, water and unconverted glycerol are considered to be recirculated within the system. The LCI values were established according to the experimental results obtained in this work at optimum conditions and are presented in the results section related to LCA (Section 3.8).

In order to analyze and compare the impact categories, the software SimaPro® 9.1.0.11 PhD was used. Inventory models for inputs were obtained from the Ecoinvent v.3 and US LCI database. The environmental potential midpoint impacts were evaluated using the CML-IA V3.06/EU25 baseline method (Center of Environmental Science of Leiden University). The assessed midpoint impact categories were: Abiotic depletion potential (ADP elements) (kg Sb eq), Abiotic depletion potential (ADP fossil fuels) (MJ), Global warming of 100 years (GWP) (kg CO<sub>2</sub> eq), Ozone layer depletion (ODP) (kg CFC-11 eq), Human toxicity

$$\eta_{CO_2} = -658.45 + 128.49x_1 + 200.84x_2 - 2.92x_3 - 0.98x_1x_2 + 1.19x_2x_3 - 9.34x_1^2 - 21.64x_2^2 - 0.02x_3^2 \quad (10)$$

(HT) (kg 1,4-DB eq), Fresh water aquatic ecotoxicity (FWAE) (kg 1,4-DB eq), Marine aquatic ecotoxicity (MAE) (kg 1,4-DB eq), Terrestrial ecotoxicity (TE) (kg 1,4-DB eq), Photochemical oxidation (PO) (kg C<sub>2</sub>H<sub>4</sub> eq), Acidification (A) (kg SO<sub>2</sub> eq) and Eutrophication (E) (kg PO<sub>4</sub> eq). The carbon footprint of the actual process (scenario 1), given by the GWP, was contrasted with a hypothetical one, the one obtained when the energy for the electrodes was provided by a solar photovoltaic system (scenario 2). The impact factor scores, expressed in millipoints (mPts), of the end-point environmental indicators for Scenarios 1 and 2 (Ecosystem Quality, Human Health Damage and Resource Availability), were calculated using ReCiPe 2016 Endpoint (H) V1.04/World (2010) H/A.

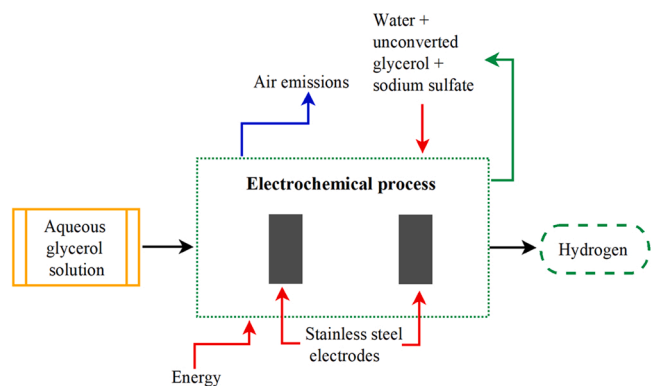


Fig. 1. System boundary for the hydrogen production by the glycerol electrochemical reforming process (cradle to gate).

### 3. Results and discussion

#### 3.1. Model fitting and ANOVA

In this work, the optimization was carried out by the RSM. Also, the Design Expert® V.10.0 software was adopted to perform the experimental design, regression analysis, equation fitting, and optimization process. The total number of experiments was thirteen (see Table S1); where runs 1, 6, 9, and 10 are factorial points; runs 2, 4, 7, 8, 11, and 13 are axial points; and runs 3, 5, and 12 are central points. The response values (hydrogen concentration ( $\eta_{CH_2}$ ) and oxygen concentration ( $\eta_{CO_2}$ )) are displayed in Table S1.

Based on the experimental values of responses reported in Table S1, the interval of hydrogen concentration and oxygen concentration are 56.0532–94.8395 mg/L and 27.3407–105.8360 mg/L, respectively. Quadratic regression model equation for the responses  $\eta_{CH_2}$  and  $\eta_{CO_2}$  are given by Eqs. (9) and (10).

In terms of uncoded variables,

$$\eta_{CH_2} = -157.35 + 58.64x_1 + 53.65x_2 - 1.60x_3 - 0.35x_1x_3 + 0.51x_2x_3 - 5.21x_1^2 - 6.42x_2^2 \quad (9)$$

In terms of coded variables

$$\eta_{CH_2} = 84.22 + 9.89X_1 + 2.32X_2 + 8.74X_3 - 7.00X_1X_3 + 10.30X_2X_3 - 5.21X_1^2 - 6.42X_2^2$$

In terms of uncoded variables,

$$\eta_{CO_2} = -658.45 + 128.49x_1 + 200.84x_2 - 2.92x_3 - 0.98x_1x_2 + 1.19x_2x_3 - 9.34x_1^2 - 21.64x_2^2 - 0.02x_3^2 \quad (10)$$

In terms of coded variables,

$$\eta_{CO_2} = 92.39 + 23.37X_1 + 0.59X_2 - 6.61X_3 - 19.64X_1X_3 + 23.80X_2X_3 - 9.34X_1^2 - 21.65X_2^2 - 6.42X_3^2$$

#### 3.2. Interaction effects between factors

In Eqs. (9) and (10), a negative sign before the  $\beta$  values of the quadratic multiple regression models in terms of coded variables suggest an unfavorable effect between operational variables, while a positive sign suggests a favorable effect [50]. Therefore, it can be seen from Eq. (9), that the hydrogen concentration increases with  $C_G$  ( $X_1$ ),  $I$  ( $X_2$ ) and  $T$  ( $X_3$ ). Also, the interaction term between glycerol concentration and temperature ( $X_1X_3$ ) had an unfavorable effect on  $\eta_{CH_2}$ , while the interaction term between the current intensity and temperature ( $X_2X_3$ ) had a favorable effect on  $\eta_{CH_2}$ . Similarly, it can be observed from Eq. (10), that the oxygen concentration increases with  $C_G$  ( $X_1$ ) and  $I$  ( $X_2$ ) but decreases with  $T$  ( $X_3$ ). Also, the interaction term between the glycerol concentration and temperature ( $X_1X_3$ ) had an unfavorable effect on  $\eta_{CO_2}$ , while the interaction term between current intensity and temperature ( $X_2X_3$ ) had a favorable effect on  $\eta_{CO_2}$ . Therefore, the concurrent increase of glycerol concentration and temperature is not advised.

#### 3.3. Analysis of variance

The quadratic regression model was used to perform an ANOVA of the experimental results for the hydrogen process, as shown in Table 4. ANOVA indicates that the quadratic models for the responses  $\eta_{CH_2}$  and

**Table 4**  
ANOVA for Response Surface Reduced Quadratic models.

Source	Sum of Squares	Degree of freedom	Mean Square	F-value	p-value	Remark
Concentration of hydrogen ( $C_{H_2}$ ), $\eta_{C_{H_2}}$ (mg/L)						
Model	1316.84	7	188.12	35.10	0.0006	significant
$X_1$	195.79	1	195.79	36.54	0.0018	
$X_2$	10.76	1	10.76	2.01	0.2156	
$X_3$	458.71	1	458.71	85.60	0.0002	
$X_1X_3$	65.38	1	65.38	12.20	0.0174	
$X_2X_3$	141.53	1	141.53	26.41	0.0036	
$X_1^2$	74.89	1	74.89	13.98	0.0135	
$X_2^2$	113.98	1	113.98	21.27	0.0058	
Residual	26.79	5	5.36			
Lack of Fit	13.50	3	4.50	0.68	0.6422	not significant
Pure Error	13.29	2	6.65			
Cor Total	1343.63	12				
$R^2 = 0.9801$ ; $R_{Adj}^2 = 0.9521$ ; $R_{Pred}^2 = 0.7634$ ; Adequate precision = 20.943; C.V. (%) = 2.94						
Concentration of oxygen ( $C_{O_2}$ ), $\eta_{C_{O_2}}$ (mg/L)						
Model	5910.3777	8	738.7972	152.2901	0.0001	significant
$X_1$	1092.6247	1	1092.6247	225.2254	0.0001	
$X_2$	0.7192	1	0.7192	0.1482	0.7198	
$X_3$	262.0807	1	262.0807	54.0233	0.0018	
$X_1X_2$	514.4447	1	514.4447	106.0438	0.0005	
$X_2X_3$	755.5296	1	755.5296	155.7392	0.0002	
$X_1^2$	222.4137	1	222.4137	45.8467	0.0025	
$X_2^2$	1195.6360	1	1195.6360	246.4594	< 0.0001	
$X_3^2$	105.051974	1	105.05197	21.6546	0.0096	
Residual	19.4049	4	4.8512			
Lack of Fit	9.5864	2	4.7932	0.98	0.5060	not significant
Pure Error	9.8186	2	4.9093			
Cor Total	5929.78	12				

$\eta_{C_{O_2}}$  were significant, as the  $p$ -value and  $F$ -value are 0.0006 and 35.10, and 0.0001 and 152.2901, for  $\eta_{C_{H_2}}$  and  $\eta_{C_{O_2}}$ , respectively. Therefore, the models are suitable for the hydrogen process ( $p$ -value < 0.05 and higher  $F$ -value) [51]. Adequate precision ratios greater than 4 indicated a very good signal [52]. For the quadratic tested models ( $\eta_{C_{H_2}}$  and  $\eta_{C_{O_2}}$ ), the adequate precision ratio of the two models were 20.943 and 42.954,

respectively, indicating that the model can be used to navigate the design space. Also, from the ANOVA, the lack-of-fit  $F$ -test was statistically not significant as the  $p$ -values were greater than 0.005 (13.50 and 9.58 for  $\eta_{C_{H_2}}$  and  $\eta_{C_{O_2}}$ , respectively), which implies a significant model correlation between variables ( $x_1$ ,  $x_2$ , and  $x_3$ ) and responses,  $\eta_{C_{H_2}}$  and  $\eta_{C_{O_2}}$ . Additionally, the  $R^2$  values were 0.9801 and 0.9967 for  $\eta_{C_{H_2}}$  and

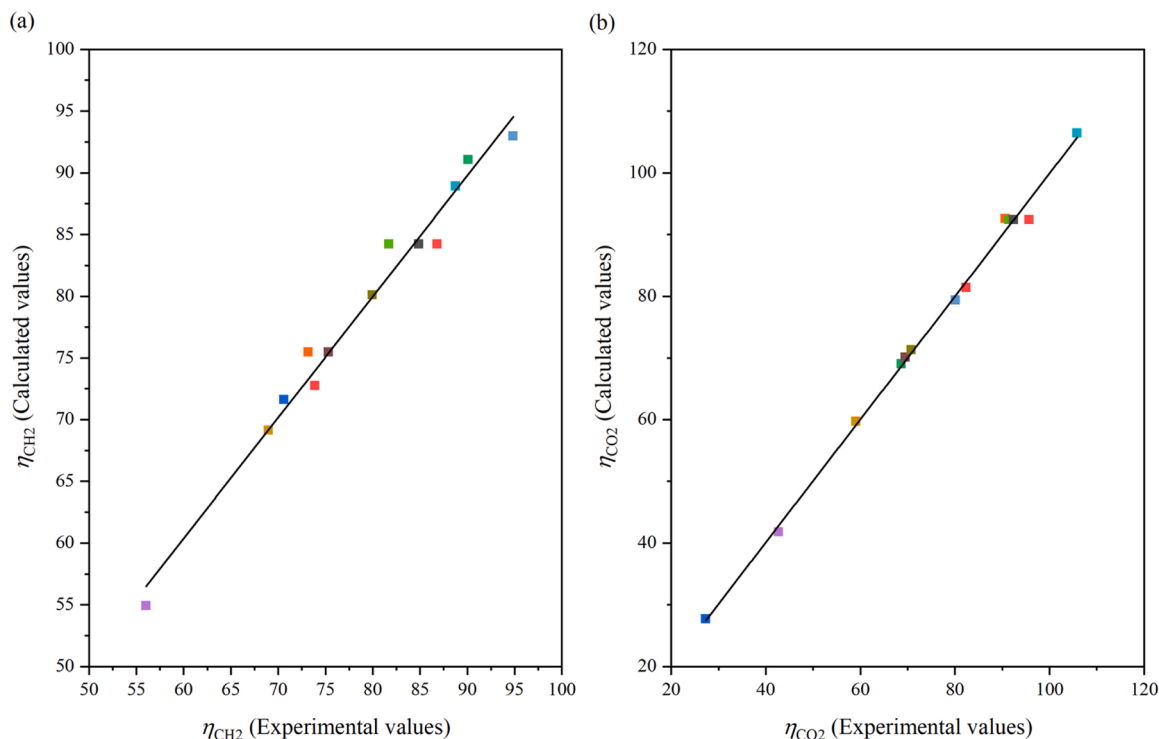


**Fig. 2.** (a) Calculated versus experimental values plot for  $\eta_{C_{H_2}}$ , and (b) Calculated versus experimental values plot for  $\eta_{C_{O_2}}$ .

$\eta_{CO_2}$ , respectively, which means that the tested models successfully fit the data because have high  $R^2$  values [53]. Also, the difference between  $R_{Adj}^2$  and  $R_{Pred}^2$  for both responses (0.1887 and 0.0663 for  $\eta_{CH_2}$  and  $\eta_{CO_2}$ , respectively) was less than 0.2, corroborating a reasonable agreement with the model fitting. Furthermore, the performance index RMSE for responses  $\eta_{CH_2}$  and  $\eta_{CO_2}$  was computed by using Eq. (8), giving values of 0.065 and 0.054 for hydrogen concentration and oxygen concentration, respectively. Small values of RMSE indicate that the developed models (Eqs.(9) and (10)) are in very good agreement with the experimental results.

$R^2 = 0.9967$ ;  $R_{Adj}^2 = 0.9902$ ;  $R_{Pred}^2 = 0.9239$ ; Adequate precision = 42.954; C.V. (%) = 2.93.

The parity plots shown in Fig. 2 are evidence of the model suitability. Fig. 2 shows there is a good quality correlation between experimental data and calculated values for both responses ( $\eta_{CH_2}$  and  $\eta_{CO_2}$ ). The small value of coefficient of variance (C.V. (%): 2.94 and 2.93 for  $\eta_{CH_2}$  and  $\eta_{CO_2}$ , respectively) exhibited the highest grade of precision of the conducted tests because the C.V. (%) of the model was lesser than 10%, then it can be concluded that the model is reproducible [47].

The perturbation diagram (Fig. 3) of the three tested operational variables ( $C_G$ ,  $I$ , and  $T$ ), showed that the current intensity was the most significant operational variable on objective function  $\eta_{CH_2}$ , while the less significant operational variable on objective function  $\eta_{CH_2}$  (Fig. 3(a)) was the temperature. Likely, it can be seen from Fig. 3(b) that the less significant variable on objective function was temperature, while the most significant factor on objective function  $\eta_{CO_2}$  was the current intensity, due to the noticeable curvature of the shape. In order to establish the impact of individual operating variables ( $x_1$ ,  $x_2$ , and  $x_3$ ) on the chosen responses ( $\eta_{CH_2}$  and  $\eta_{CO_2}$ ), a sensitivity analysis was performed according to Eq. (11) [54],

$$S_{x_i} = \frac{\partial \eta}{\partial x_i} \frac{x_i}{\eta(x_i)} \quad (11)$$

where  $S_{x_i}$  is the sensitivity regarding the independent operational variable  $x_i$  and  $\eta$  is the chosen responses (dependent variables).

The results of the sensitivity index ( $S_{x_i}$ ) are reported in Table 5. It can

**Table 5**

Values of sensitivity index for responses ( $\eta_{CH_2}$  and  $\eta_{CO_2}$ ).

Variable	Hydrogen concentration ( $\eta_{CH_2}$ )	Oxygen concentration ( $\eta_{CO_2}$ )
	$S_{x_i}$	$S_{x_i}$
$x_1$	0.4525	1.2123
$x_2$	0.9049	2.4245
$x_3$	0.3771	1.0102

be seen that all obtained values of sensitivity index are higher than 0.25, demonstrating that the chosen operational variables included in the fitted models (Eqs. (9) and (10)) have a noticeable effect on both objective functions ( $\eta_{CH_2}$  and  $\eta_{CO_2}$ ).  $S_{x_1}$  and  $S_{x_3}$  can be considered as very significant variables for responses  $\eta_{CO_2}$  and  $\eta_{CH_2}$ , respectively, while  $S_{x_2}$  must be considered as an extremely significant variable for responses  $\eta_{CO_2}$  and  $\eta_{CH_2}$ , respectively [55].

### 3.4. Optimization of hydrogen production

The optimal operating conditions to achieve the maximum hydrogen concentration and the minimum oxygen concentration, were determined by using the models given by Eqs. (9) and (10), and were calculated employing the multi-objective optimization method. To accomplish the optimization process, the Design-Expert ® V. 10 software was used. Additional software input information is provided in Table 6. For this case study, a default importance for all objective functions was assumed, namely all variables and objective functions have equally importance set as (+++).

**Table 6**

Constrain criteria for optimization of the hydrogen process.

Response	Objective	Min	Max	Importance
$C_G$ (mol/L)	Is in range	2.0	4.0	+++
$I$ (A)	Is in range	5.0	7.0	+++
$T$ (°C)	Is in range	30.0	70.0	+++
$\eta_{CH_2}$ (mg/L)	Maximum	56.05	94.84	+++
$\eta_{CO_2}$ (mg/L)	Minimum	27.34	105.84	+++

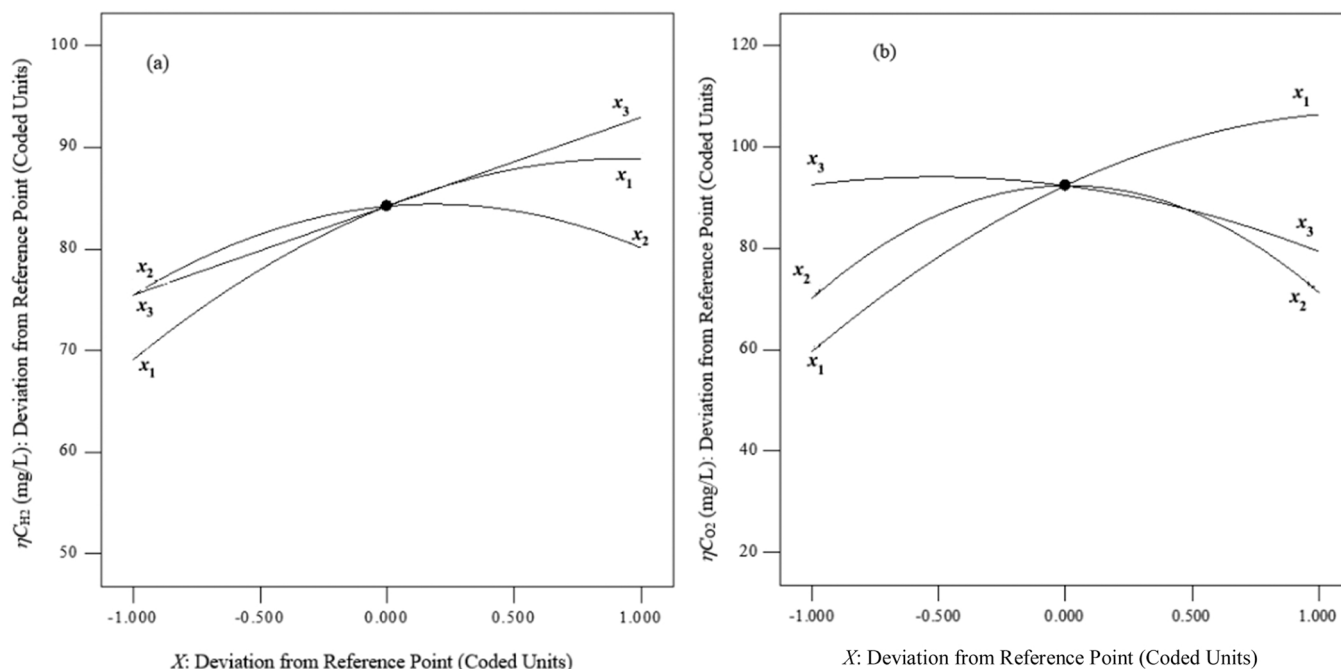


**Fig. 3.** (a) Perturbation diagram for  $\eta_{CH_2}$  (b) Perturbation diagram for  $\eta_{CO_2}$ .

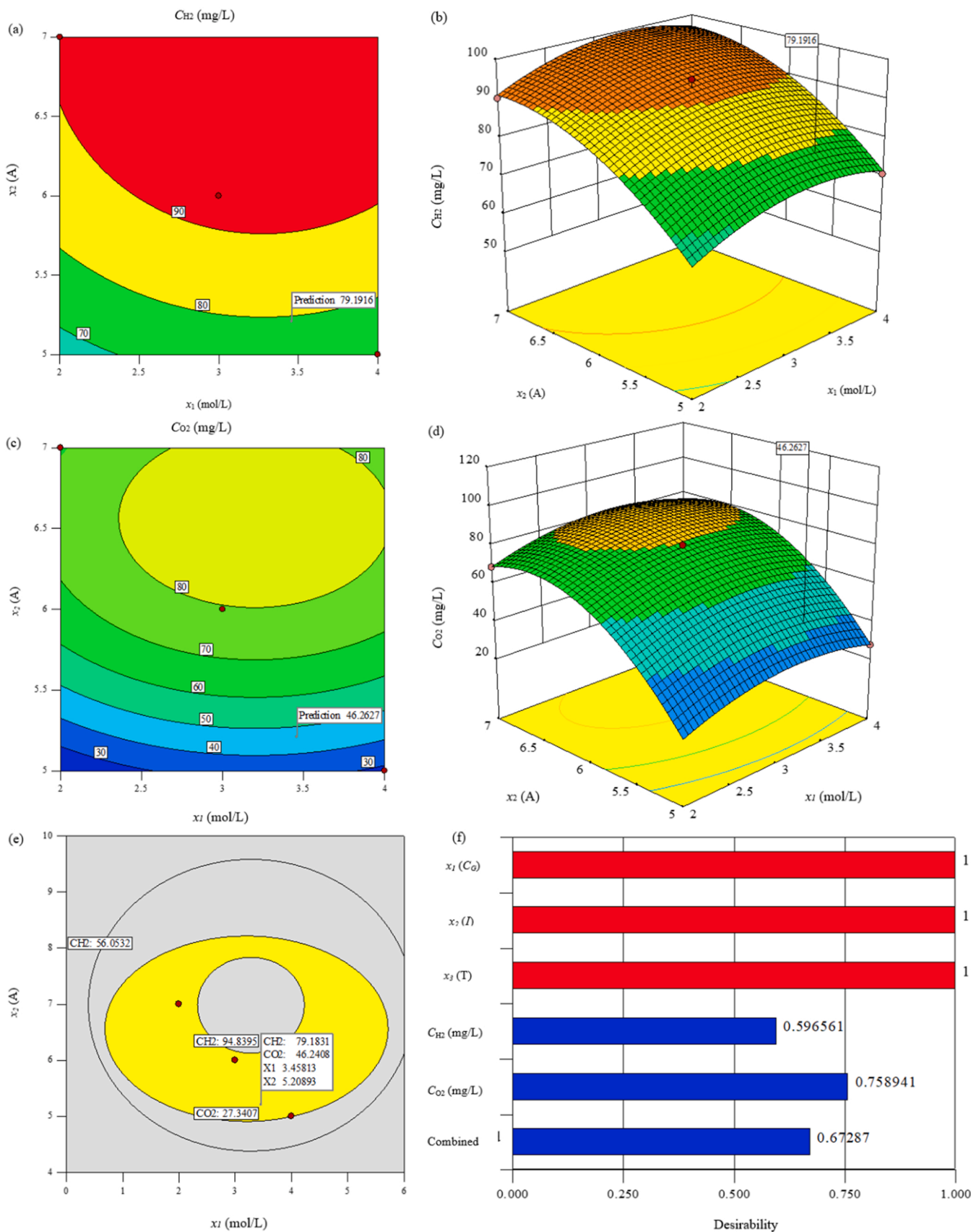


Fig. 4. (a) Contour plot for response  $\eta_{CH_2}$  concerning  $C_G$  and  $I$ ; (b) 3D plot  $\eta_{CH_2}$  concerning  $C_G$  and  $I$ ; (c) Contour plot for  $\eta_{CO_2}$  concerning  $C_G$  and  $I$ ; (d) 3D plot for response  $\eta_{CO_2}$  concerning  $C_G$  and  $I$ ; (e) Optimal region plot concerning  $C_G$  and  $I$ ; (f) Bar chart of desirability. All plots were edited at a temperature of 70 °C.



Fig. 4(b) and 4(d) represent the 3D response surfaces, which were obtained by plotting Eqs. (3) and (4), respectively. These graphs allow to examine the behavior of the whole studied system from a qualitative point of view. Fig. 4(b) and 4(d) show that when the current intensity and the glycerol concentration increases, the hydrogen concentration and the oxygen concentration also increase. In addition, Fig. 4(a) and 4(c) exhibit an ellipsoid contours shape. The hydrogen concentration has a maximum point (79.19 mg/L) while the oxygen concentration has a saddle point (42.26 mg/L); which were achieved at  $C_G$  of 3.46 mol/L,  $I$  of 5.21 A, and  $T$  of 70 °C, with global desirability of 67.29% (see Fig. 4 (f)).

Fig. 4(e) illustrates the feasible operating region, which was drawn using the constrained criteria assumed (Table 5) and the responses ( $\eta_{C_{H_2}}$  and  $\eta_{C_{O_2}}$ ). The multi-optimal  $\eta_{C_{H_2}}$  and  $\eta_{C_{O_2}}$  were 79.18 mg/L and 45.26/L, respectively, at an electrolysis time of 40 min. The black lines in Fig. 4(e) denote the constraints criteria, the area that is filled in yellow represents the feasible region zone, and the region that does not convene the constraints is filled in grey. The optimal region conditions are covered by the glycerol concentration (0.6–5.7 mol/L) and the current intensity (4.88–8.2 A) at the electrolysis time of 40 min

### 3.5. Model validation

The set of operating reaction conditions with the highest value of desirability (67.28%) was considered as the optimum, for the responses  $\eta_{C_{H_2}}$  and  $\eta_{C_{O_2}}$ . To validate the proposed models, Eqs. (9) and (10), three complementary trials were performed by employing the optimal operating variables calculated with the Design-Expert® V.10 software.  $\eta_{C_{H_2}}$  and  $\eta_{C_{O_2}}$  modeled and experimental values are shown in Table 7. The small percentage errors corroborate the effectiveness of the optimization process. The conversion of glycerol into hydrogen was 39.1% at optimal operating reaction conditions ( $C_G$  of 3.46 mol/L,  $I$  of 5.21 A, and  $T$  of 70 °C at reaction time of 80 min).

Also, three additional experiments to produce hydrogen using different glycerol sources ([43–45]) at the optimal operating conditions found in this work were performed (see Table S2). In these experiments, it was observed that hydrogen concentration oscillates between 70.45 and 78.03 mg/L. Furthermore, the average difference on hydrogen concentration was of only 6% when using commercial glycerol and waste glycerol. Therefore, the process employed in this work could be a promising process to produce green energy ( $H_2$ ) in a BSETR equipped with stainless steel electrodes since the main objective is to produce hydrogen and not added-value chemicals.

Additional analysis of the liquid-phase, at the end of the 80 min operation, indicated very low organic compounds concentrations, with the highest value for formaldehyde (0.013 mol/L, see Table S3). TOC analysis (6001 TOC analyzer Shimadzu) indicated a high inorganic content of the liquid. Thus, the carbon from glycerol oxidation was recovered as dissolved  $CO_2$  (1008.248 mg/L, see Table S4) or gaseous  $CO_2$  (135.89 mg/L, measured in an Agilent 6890 gas chromatograph). The main products of reaction in the gas-phase were  $H_2$ ,  $O_2$  and  $CO_2$ .

**Table 7**  
Optimal operating conditions of the hydrogen process.

Operating variables	Value	Responses	Values		
			Modeled	Experimental	Percentage error
$C_G$ (mol/L)	3.46				
$I$ (A)	5.21	$\eta_{C_{H_2}}$ (mg/L)	79.18	78.03	1.47%
$T$ (°C)	70.0	$\eta_{C_{O_2}}$ (mg/L)	46.24	45.26	2.16%

### 3.6. Glycerol conversion, $H_2$ yield, and $H_2$ selectivity

In Table 8, the glycerol conversion (liquid-phase and gas-phase),  $H_2$  yield, and  $H_2$  selectivity in the gas-phase are reported. These values were calculated according to Eqs. (S1) to (S4). In this figure the glycerol conversion in liquid-phase is lower (13.29%) for the electrochemical reforming process than the other referenced processes (between 84% and 100%) but the reaction time was also lower (80 min) than the other processes (between 120 and 1800 min). Also, the best hydrogen selectivity (5.49) was achieved with the electrochemical reforming process. Additionally, the best hydrogen yield achieved was with the aqueous-phase reforming, but the treated volume is lower (6 mL) than steam reforming (1370 mL) and electrochemical reforming (500 mL). Moreover, the liquid-phase conversion reached in this work was similar to than reported in literature (19.3 [18] and 15.6 [56]). Based on the above, the electrochemical reforming of glycerol could be a promising technology when the process operates at long reaction times in order to increase the glycerol conversion,  $H_2$  yield, and  $H_2$  selectivity.

### 3.7. Total operational cost

The total operational cost (*TotalOC*) of the hydrogen production by electrochemical reforming of aqueous glycerol solution involves the specific energy consumption ( $E_{con}$  (kWh/kg  $H_2$ )), electrode material cost ( $c_{electrode}$  (kg/kg  $H_2$ )), and the electrolyte cost ( $c_{electrolyte}$  (kg/kg  $H_2$ )). The total operational cost for the hydrogen production process can be estimated by a set of Eqs. (12)–(15) [60,61].

$$E_{con} = \frac{U_{cell} I t_{rxn}}{Mass_{H_2}} \quad (12)$$

$$c_{electrode} = \frac{I t_{rxn} M}{z F Mass_{H_2}} \quad (13)$$

$$c_{electrolyte} = \frac{q_{Na_2SO_4}}{Mass_{H_2}} \quad (14)$$

$$TotalOC = \alpha E_{con} + \xi c_{electrode} + \phi c_{electrolyte} \quad (15)$$

where  $\alpha$  is the electrical energy price in Mexico (0.043 USD\$/kWh supplied by Federal Electricity Commission (CFE), considering that 1 USD/20 MXP),  $\xi$  is electrode price (5.51 USD\$/kg of stainless steel) for the Mexican market in 2021,  $\phi$  is the price of electrolyte (0.43 USD\$/kg, supplied by Karal S.A. de C.V., Mexican Company),  $q_{Na_2SO_4}$  is the quantity of external chemical used (kg),  $U_{cell}$  is the average cell potential (V),  $I$  is the current intensity (A),  $t_{rxn}$  is the reaction time (h),  $M$  is the molecular mass of the iron (g/mol),  $Mass_{H_2}$  is the hydrogen mass generated,  $z$  is the number of electrons transferred ( $z = 2$ ), and  $F$  is the Faraday constant (96,485 C/mol).

Based on the set of Eqs. (12)–(15), the TOC of the hydrogen production process employed in this work was 2.74 USD\$/kg  $H_2$  when the experimental system was operated at optimum conditions ( $T = 70$  °C,  $C_G = 3.46$  mol/L, and  $I = 5.21$  A, at electrolysis time of 80 min).

Table 9 shows the energy consumption of different electrochemical reforming environments to produce hydrogen employing glycerol as carbon-based fuel. In this table, optimized refers to those studies where an optimization process was carried out while non-optimized refers to those studies where a systematic study was conducted and only the best conditions within the studied range, are reported. It can be observed in Table 9 that the energy consumption for the present process is 40.72 kWh/kg  $H_2$ , i.e., 9.51% less than for the water electrolysis (45 kWh/Kg  $H_2$ ) and 18.56–25.96% less than the commercial water electrolysis (50–55 kWh/Kg  $H_2$ ). It is worth noting that the present work is the only one that performs a process optimization and provides the TOC (2.74 USD\$/kg  $H_2$ ) of the hydrogen production process employed here, which is highly competitive since the cost of the commercial Polymer Electrolyte Membrane (PEM) electrolysis system is of 5–6 USD\$/kg  $H_2$  [62].

**Table 8**Glycerol conversion, hydrogen yield, and hydrogen selectivity of H<sub>2</sub> production with different processes.

Process	Volume (mL)	Time (min)	Conversion (%)		H <sub>2</sub> yield	H <sub>2</sub> selectivity	Reference
			Liquid-phase	Gas-phase			
Electrochemical reforming of Glycerol	500	80	13.29	0.103	0.012	5.49	[This work]
Autothermal reforming of Glycerol	–	1800	100.00	–	0.25	–	[57]
Aqueous-phase reforming of glycerol	6	120	84.00	–	0.65	3.35	[58]
Steam reforming of crude glycerol	1370	840	96	–	0.070	–	[59]
Electrochemical reforming of Glycerol	–	600	19.30	–	–	–	[18]
Electrocatalytic dehydrogenation of glycerol	–	–	34.2	–	–	–	[56]
Electrochemical reforming of Glycerol	–	–	15.6	–	–	–	[34]

**Table 9**

Electrochemical reforming of glycerol to hydrogen production under various operational reaction environments.

Operating environments		Compared data				
Optimized	Non-Optimized	Anode/ Cathode	Reactor volume (cm <sup>3</sup> )	E <sub>con</sub> (kWh/kg H <sub>2</sub> )	Total OC (USD\$/Kg H <sub>2</sub> )	Ref.
*	*	*/(Pt/C)	–	50–55	–	[63,64]
**	**	***/(Pt/C)	–	45	–	[65,66]
	90 °C, 0.7 V, 0.015 A, C <sub>G</sub> = 1 mol/L, and 24 h	a/(Pt/C)	10	22	–	[31]
	70 °C, C <sub>G</sub> = 8.5 mol/L, and 0.48–0.7 V	b/Pt	–	12.24	–	[16]
	40 °C, C <sub>G</sub> = 10% wt, 0.7 V, and 15 h	c/(Pt/C)	150	22.24	–	[67]
	75 °C, C <sub>G</sub> = 4 mol/L, 1 V, 2 A/cm <sup>2</sup> , and 20 min	d/(Pt/C)	–	20	–	[33]
	60 °C, 474 mA/cm <sup>2</sup> , C <sub>G</sub> = 2 mol/L,	d/(Pt/C)	30	15.9	–	[68]
	80 °C, 200 mA/cm <sup>2</sup> , C <sub>G</sub> = 1 mol/L, and 10 h	PtRu/(Pt/C)	250	36	–	[69]
70 °C, C <sub>G</sub> = 3.46 mol/L, 5.21 A, and 40 min		SS/SS	640	40.72	2.74	This work

\* : Commercial water electrolysis; \* \*: Water electrolysis process; a: Pd3Bi/C; b: RuO<sub>2</sub>/IrO<sub>2</sub>; c: Pd-(Ni-Zn)/C; d: Pd-CeO<sub>2</sub>/C; SS: Stainless steel.**Table 10**

Inventory data to produce 1MJ of hydrogen.

Inventory item	Input	Output	Unit	Data quality
Glycerol	4.32	–	kg	Experimental
Deionized water	52.62	62.62	kg	Experimental
Sodium sulfate (Na <sub>2</sub> SO <sub>4</sub> )	0.0037	0.0037	kg	Experimental
Stainless steel electrodes	0.08	–	kg	Experimental
Electricity consumption	0.34	–	kWh	Experimental
Hydrogen	–	1	MJ	Experimental
Oxygen	–	0.0024	kg	Experimental

**Table 11**

Midpoint environmental impacts of 1MJ of hydrogen.

Impact categories	Unit	Total
ADP (elements)	kg Sb eq	9.81 × 10 <sup>-6</sup>
ADP (fossil fuels)	MJ	6.52
GWP	kg CO <sub>2</sub> eq	0.192
ODP	kg CFC-11 eq	1.36 × 10 <sup>-8</sup>
HT	kg 1, 4-DB eq	0.025
FWAE	kg 1, 4-DB eq	3.54 × 10 <sup>-3</sup>
MAE	kg 1, 4-DB eq	53.52
TE	kg 1, 4-DB eq	4.50 × 10 <sup>-4</sup>
PO	kg C <sub>2</sub> H <sub>4</sub> eq	3.14 × 10 <sup>-5</sup>
A	kg SO <sub>2</sub> eq	7.75 × 10 <sup>-4</sup>
E	kg PO <sub>4</sub> eq	7.86 × 10 <sup>-5</sup>

### 3.8. Life cycle assessment

The goal of this assessment was to evaluate the environmental impacts of producing hydrogen by the electrochemical reforming of glycerol at optimum conditions under two scenarios, when the electrodes are energized by electricity from fossil fuels (scenario 1) and that from a solar photovoltaic system (scenario 2). The selected FU was the production of 1MJ of energy from H<sub>2</sub>. According to literature, the mass of

H<sub>2</sub> necessary to provide 1 MJ, is  $8.3 \times 10^{-3}$  kg. The system boundary is depicted in Fig. 2. Based on this system, the LCI for the hydrogen production at optimum conditions was established. There is in Table 10, the summary of inputs and outputs associated with the production of the FU at optimum conditions.

With the inventory data presented in Table 10, the midpoint environmental impacts of the hydrogen production by electrochemical reforming of glycerol were evaluated and are summarized in Table 11. As can be seen in this table, there are three impact categories mainly affected, MAE, ADP (fossil fuels) and GWP. MAE (marine aquatic ecotoxicity) refers to the impact related to the discharge of toxic compounds into the aquatic ecosystems and its units are equivalent kg of 1,4 dichlorobenzene (1,4-DB). ADP (fossil fuels) expresses the depletion of not alive natural resources such as carbon, oil, natural gas, gasoline and minerals like iron and antimony and therefore its units are Sb equivalent kg. GWP indicates the impact of the anthropogenic emissions on the absorption of calorific radiation by the atmosphere, thus causing an

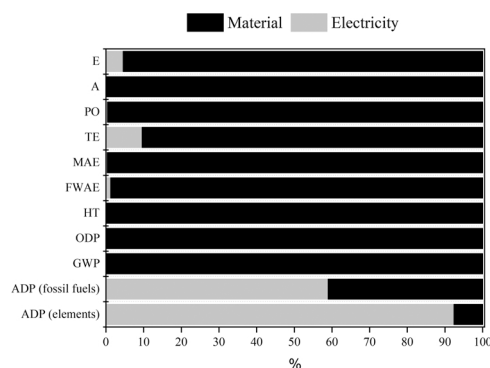


**Fig. 5.** Contribution analysis for the electrochemical reforming of glycerol into hydrogen.

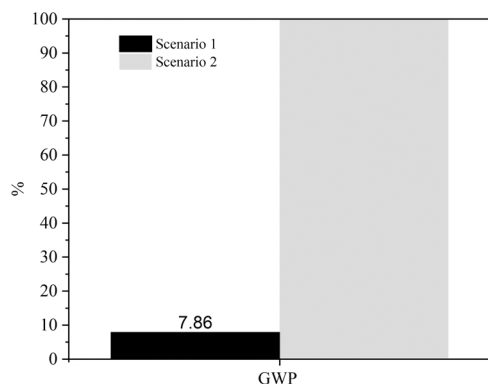


**Fig. 6.** Effect of the energy source on the Global Warming Potential impact category. Scenarios: fossil fuels (Scenario 1) and solar photovoltaic system (Scenario 2).

increase in the planet temperature (i.e. global warming) and is given in equivalent carbon dioxide kilograms. This is an important indicator of the sustainability of a process, especially when the process is related to the production of fuels or energy.

In order to establish the source of these impacts, an environmental contribution analysis was conducted, and the results are shown in Fig. 5. According to these results, the highest contribution to the midpoint impact categories, 2.82–100%, is a consequence of the electricity consumption. Thus, it can be concluded that in order to reduce the environmental impact on MAE, E, A, PO, TE, FWAE, HT, ODP and GWP, the electricity consumption produced by non-renewable energy sources must be minimized or eliminated. Since the base of this process is electrochemical, the way to reduce these impacts is by using an alternative source of energy such as a solar photovoltaic system. Thus, this scenario is below analyzed but only in terms of its impact on the carbon footprint of the process or GWP. As can be seen in Fig. 6, the electrodes material (stainless steel) has an important contribution to the impact categories of ADP (elements) and ADP (fossil fuels) between (61.26–97.18%) as a result of the steelmaking process. Therefore, from the contribution analysis presented in Fig. 6, it can be concluded that the electrodes material mainly contributes to the ADP (elements) and ADP (fossil fuels) midpoint impact categories. In addition, the electrodes material will also indirectly affect the other categories by modifying the energy consumption and process efficiency.

In the interpretation stage, two scenarios regarding energy were compared according to different sources of electricity, fossil fuels (scenario 1) and solar PV (scenario 2). It was found that, as expected, if a solar PV system is coupled to the electrochemical process, the GWP impact, i.e., carbon footprint will be reduced around 92.1% (0.0151 kg CO<sub>2</sub> eq/MJ H<sub>2</sub>) (see Fig. 6). The PV system also represents a potential cost reduction and efficiency improvement of the hydrogen production by the process presented here.

The literature related to the assessment of environmental impacts of electrochemical reforming of glycerol is scarce. Thus, there are summarized in Table 12 the values of global warming potential of the hydrogen production with the assessed technology in this study and with other technologies, like water electrolysis, steam methane reforming, glycerol autothermal reforming, glycerol steam reforming and alcohols reforming. In this context, it can be concluded that the process herein studied shows an improved global warming potential compared to other processes like glycerol autothermal reforming, and glycerol supercritical water reforming. Nevertheless, the sustainability of the electrochemical reforming of glycerol studied here (entry 1) is not competitive with that of the steam methane reforming (entry 10) or glycerol aqueous phase reforming (entry 11). This can be mainly ascribed to the source of the electrical energy in each process. Therefore, this completely changes when a solar photovoltaic system is used to provide the required energy

**Table 12**

Global warming potential as a function of the process to produce hydrogen.

Entry	Process	Feedstock energy	Electricity (kWh/kg H <sub>2</sub> )	GWP (Kg CO <sub>2</sub> eq)/kgH <sub>2</sub>	Ref.
1	Electrochemical reforming of glycerol	Fossil fuels	40.72	23.04	This work
2	Electrochemical reforming of glycerol	Solar	NA	1.81	
3	PEM, H <sub>2</sub> O electrolysis	Fossil fuels	54.16	29.54	[70]
4	PEM, H <sub>2</sub> O electrolysis	Wind	NA	2.21	
5	SOEC	Fossil fuels	36.14	23.32	[71]
6	SOEC	Wind	NA	5.10	
7	Electrolysis	Wind	54.2	0.86	[72]
8	Electrolysis	Solar	54.2	3.1	
9	Electrolysis	Nuclear	54.2	0.67	
10	Steam methane reforming	Natural gas	NA	9	[73]
11	Glycerol aqueous phase reforming	Scenario with electricity generation from the US electricity-grid	NA	4.1	[74]
12	Glycerol autothermal reforming			87.2	
13	SCWR			51.9	
14	Glycerol steam reforming (GSR)	Fossil fuels	0.49	12.65	[75]
15	Ethanol reforming	NA	NA	12.2	[76]
16	Methanol reforming	NA	NA	17.9	

NA: Data not available; SOEC: Solid oxide electrolysis cells; SCWR: Glycerol supercritical water reforming; PEM: Proton exchange membrane; GSR: Glycerol steam reforming.

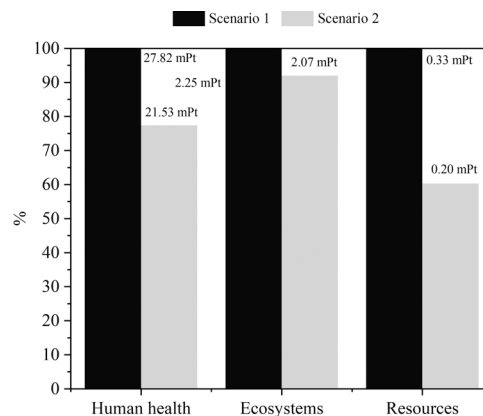


**Fig. 7.** Effect of the source of energy on the end point impact categories. Scenarios of energy consumption: Fossil fuels (1) and Solar photovoltaic system (2). Impact factors score in mPts.

for the electrodes to work (entry 2). Entries 7, 8 and 9 suggest that by using other renewable sources of energy, such as wind or nuclear, makes possible a further reduction in GWP of the electrochemical reforming of glycerol.

Fig. 7. presents the end point impact categories for scenarios 1 and 2. It can be observed that unlike in the GWP, the scenario 2 does not minimize none of the impact categories. This is due to the presence of the electrodes that importantly contribute to each impact category and therefore this cannot be eliminated in any electrochemical system. In addition, these environmental impacts for scenario 2, are also due to the manufacturing process and material of the solar panels in the PV system. Therefore, the use of other materials than crystalline silicon has been

reported [72] as a strategy to reduce further the environmental impacts of using solar panels.

#### 4. Conclusions

In this work, the electrochemical reforming of aqueous glycerol-water and waste glycerol-water mixtures was successfully carried out in a BSRTR equipped with stainless steel electrodes (both as cathode and anode) and a 13.12% of glycerol conversion was achieved after 80 min of reaction time.

The quadratic model to predict the hydrogen concentration from the glycerol electrochemical reforming with stainless steel electrodes is,

$$\eta_{C_{H_2}} = 84.22 + 9.89X_1 + 2.32X_2 + 8.74X_3 - 7.00X_1X_3 + 10.30X_2X_3 - 5.21X_1^2 - 6.42X_2^2$$

The optimization of operational variables was successfully attained through RSM based on face-centered central composite design. Maximum hydrogen (79.18 mg/L) and minimum oxygen (46.24 mg/L) concentrations were achieved at operating conditions of  $C_G = 3.46$  mol/L,  $I = 5.21$  A, and  $T = 70$  °C, at electrolysis time of 80 min with an  $E_{con}$  of 40.72 kWh/kg  $H_2$  and TOC of 2.74 USD\$/kg  $H_2$ . The sensitivity analysis demonstrates that variable  $x_2$  (current intensity) is an extremely significant variable for both responses ( $\eta_{C_{O_2}}$  and  $\eta_{C_{H_2}}$ ), while the concurrent increase of glycerol concentration and temperature is detrimental for the hydrogen production.

The carbon footprint of the hydrogen production by the optimized process is 0.192 kg  $CO_2$  eq. This footprint is due to the use of fossil fuels as the source of energy for the electrodes (scenario 1) and therefore such a carbon footprint can be reduced around 92.1% if solar PV energy (scenario 2) is used instead. Regarding the end point impact categories, scenario 2, compared to scenario 1, improves the impact on human health 22.61%, on ecosystems 8% and on resources 39.39%.

The hydrogen production process assessed in this work, is a promising green energy technology as it uses waste glycerol as a carbon-based fuel and a low-cost anode material (7.5 USD¢/kg  $H_2$ ) as stainless steel.

#### CRedit authorship contribution statement

**Ever Peralta-Reyes:** Supervision, Methodology, Writing – review & editing, Resources. **Diego Vizarratea-Vásquez:** Investigation, Validation. **Reyna Natividad:** Conceptualization, Writing – review & editing, Software SimaPro. **Aitor Aizpuru:** Data curation, Writing – review & editing, Resources. **Edson Robles-Gómez:** Conceptualization, Writing – review & editing, Resources. **Claudia Alanis:** Conceptualization, Software SimaPro, Writing – review & editing. **Alejandro Regalado-Méndez:** Supervision, Methodology, Investigation, Formal analysis, Writing – original draft preparation, Software Design Expert. All authors have read and agreed to the published version of the manuscript.

#### Declaration of Competing Interest

The authors declare that they have no known competing financial interests or personal relationships that could have appeared to influence the work reported in this paper.

#### Acknowledgments

This work was supported by the internal project of Universidad del Mar, Puerto Ángel, Oaxaca, México (Grant No. CUP: 2II2104).

#### Appendix A. Supporting information

Supplementary data associated with this article can be found in the online version at [doi:10.1016/j.jece.2022.108108](https://doi.org/10.1016/j.jece.2022.108108).

#### References

- [1] B. Holmatov, J.F. Schyns, M.S. Krol, P.W. Gerbens-Leenes, A.Y. Hoekstra, Can crop residues provide fuel for future transport? Limited global residue bioethanol potentials and large associated land, water and carbon footprints, *Renew. Sustain. Energy Rev.* 149 (2021), 111417, <https://doi.org/10.1016/j.rser.2021.111417>.
- [2] C. Chen, A. Chitose, M. Kusadokoro, H. Nie, W. Xu, F. Yang, S. Yang, Sustainability and challenges in biodiesel production from waste cooking oil: an advanced bibliometric analysis, *Energy Rep.* 7 (2021) 4022–4034, <https://doi.org/10.1016/j.jegyr.2021.06.084>.
- [3] D.D.T. Ferraren-De Cagalitan, M.L.S. Abundo, A review of biohydrogen production technology for application towards hydrogen fuel cells, *Renew. Sustain. Energy Rev.* 151 (2021), 111413, <https://doi.org/10.1016/j.rser.2021.111413>.
- [4] A. Saeedmanesh, M.A. Mac Kinnon, J. Brouwer, Hydrogen is essential for sustainability, *Curr. Opin. Electrochem.* 12 (2018) 166–181, <https://doi.org/10.1016/j.coelec.2018.11.009>.
- [5] M. Noussan, P.P. Raimondi, R. Scita, M. Hafner, The role of green and blue hydrogen in the energy transition—a technological and geopolitical perspective, *Sustainability* 13 (2021), <https://doi.org/10.3390/su13010298>.
- [6] B. Ipek, I. Altıparmak, Remarkable isosteric heat of hydrogen adsorption on Cu(I)-exchanged SSZ-39, *Int. J. Hydrog. Energy* 45 (2020) 34972–34982, <https://doi.org/10.1016/j.ijhydene.2020.03.083>.
- [7] M. Martino, C. Ruocco, E. Meloni, P. Pullumbi, V. Palma, Main hydrogen production processes: an overview, *Catalysts* 11 (2021), <https://doi.org/10.3390/catal11050547>.
- [8] O. Alizadeh Sahraei, A. Desgagnés, F. Larachi, M.C. Iliuta, A comparative study on the performance of M (Rh, Ru, Ni)-promoted metallurgical waste driven catalysts for  $H_2$  production by glycerol steam reforming, *Int. J. Hydrog. Energy* (2021), <https://doi.org/10.1016/j.ijhydene.2021.06.192>.
- [9] N. Hamed, S. Masoumi, M. Nategh, M.R. Rahimpour, Simultaneous production of xylenes and hydrogen in an optimized membrane-assisted thermally coupled reactor using an elaborate reaction network, *Chem. Eng. Process. Intensif.* 119 (2017) 113–130, <https://doi.org/10.1016/j.ccep.2017.05.011>.
- [10] A. De Lucas-Consuegra, J. González-Cobos, Y. Gacia-Rodríguez, J.L. Endrino, J. L. Valverde, Electrochemical activation of the catalytic methanol reforming reaction for  $H_2$  production, *Electrochem. Commun.* 19 (2012) 55–58, <https://doi.org/10.1016/j.elecom.2012.03.016>.
- [11] M.M. Habashy, E.S. Ong, O.M. Abdeldayem, E.G. Al-Sakkari, E.R. Rene, Food waste: a promising source of sustainable biohydrogen fuel, *Trends Biotechnol.* (2021), <https://doi.org/10.1016/j.tibtech.2021.04.001>.
- [12] Y. Lim, D.-K. Lee, S.M. Kim, W. Park, S.Y. Cho, U. Sim, Low dimensional carbon-based catalysts for efficient photocatalytic and photo/electrochemical water splitting reactions, *Materials* 13 (2020), <https://doi.org/10.3390/ma13010114>.
- [13] N. Akhlaghi, G. Najafpour-Darzi, A comprehensive review on biological hydrogen production, *Int. J. Hydrog. Energy* 45 (2020) 22492–22512, <https://doi.org/10.1016/j.ijhydene.2020.06.182>.
- [14] L. Fan, A. Mokhov, S.A. Saadabadi, N. Brandon, P.V. Aravind, Methane steam reforming reaction in solid oxide fuel cells: influence of electrochemical reaction and anode thickness, *J. Power Sources* 507 (2021), 230276, <https://doi.org/10.1016/j.jpowsour.2021.230276>.
- [15] Z. Ying, Z. Geng, X. Zheng, B. Dou, G. Cui, Optimization of anode performance in the ethanol electrochemical reforming for clean hydrogen production, *Int. J. Hydrog. Energy* 46 (2021) 119–133, <https://doi.org/10.1016/j.ijhydene.2020.09.265>.
- [16] A.T. Marshall, R.G. Haverkamp, Production of hydrogen by the electrochemical reforming of glycerol–water solutions in a PEM electrolysis cell, *Int. J. Hydrog. Energy* 33 (2008) 4649–4654, <https://doi.org/10.1016/j.ijhydene.2008.05.029>.
- [17] S. Authayanun, W. Wiyaratn, S. Assabumrungrat, A. Arpornwichanop, Theoretical analysis of a glycerol reforming and high-temperature PEMFC integrated system: hydrogen production and system efficiency, *Fuel* 105 (2013) 345–352, <https://doi.org/10.1016/j.fuel.2012.07.036>.
- [18] M. Hunsom, P. Sails, Electrochemical conversion of enriched crude glycerol: effect of operating parameters, *Renew. Energy* 74 (2015) 227–236, <https://doi.org/10.1016/j.renene.2014.08.008>.
- [19] J. Kaur, A.K. Sarma, M.K. Jha, P. Gera, Valorisation of crude glycerol to value-added products: perspectives of process technology, economics and environmental issues, *Biotechnol. Rep.* 27 (2020), e00487, <https://doi.org/10.1016/j.btre.2020.E00487>.
- [20] S.A.N.M. Rahim, C.S. Lee, F. Abnisa, M.K. Aroua, W.A.W. Daud, P. Cognet, Y. Pèrès, A review of recent developments on kinetics parameters for glycerol electrochemical conversion – a by-product of biodiesel, *Sci. Total Environ.* 705 (2020), 135137, <https://doi.org/10.1016/j.scitotenv.2019.135137>.
- [21] A. Mendoza, R. Romero, G.P. Gutiérrez-Cedillo, G. López-Tellez, O. Lorenzo-González, R.M. Gómez-Espinosa, R. Natividad, Selective production of dihydroxyacetone and glyceraldehyde by photo-assisted oxidation of glycerol, *Catal. Today* 358 (2020) 149–154, <https://doi.org/10.1016/j.cattod.2019.09.035>.
- [22] Z. Zhang, L. Xin, W. Li, Electrocatalytic oxidation of glycerol on Pt/C in anion-exchange membrane fuel cell: Cogeneration of electricity and valuable chemicals, *Appl. Catal. B Environ.* 119–120 (2012) 40–48, <https://doi.org/10.1016/j.apcatb.2012.02.009>.
- [23] G.G. Muciño, R. Romero, A. Ramírez, S.L. Martínez, R. Baeza-Jiménez, R. Natividad, Biodiesel production from used cooking oil and sea sand as heterogeneous catalyst, *Fuel* 138 (2014) 143–148, <https://doi.org/10.1016/j.fuel.2014.07.053>.
- [24] H. Luo, J. Barrio, N. Sunny, A. Li, L. Steier, N. Shah, I.E.L. Stephens, M.-M. Titirici, Progress and perspectives in photo- and electrochemical-oxidation of biomass for

- sustainable chemicals and hydrogen production, *Adv. Energy Mater.* 11 (2021) 1–51, <https://doi.org/10.1002/aenm.202101180>.
- [25] N. Gutiérrez-Guerra, M. Jiménez-Vázquez, J.C. Serrano-Ruiz, J.L. Valverde, A. de Lucas-Consegra, Electrochemical reforming vs. catalytic reforming of ethanol: a process energy analysis for hydrogen production, *Chem. Eng. Process. Process. Intensif.* 95 (2015) 9–16, <https://doi.org/10.1016/j.ccep.2015.05.008>.
- [26] K.-E. Guima, L.M. Alencar, G.C. da Silva, M.A.G. Trindade, C.A. Martins, 3D-printed electrolyzer for the conversion of glycerol into tartronate on Pd nanocubes, *ACS Sustain. Chem. Eng.* 6 (2018) 1202–1207, <https://doi.org/10.1021/acssuschemeng.7b03490>.
- [27] Y.X. Chen, A. Lavacchi, H.A. Miller, M. Bevilacqua, J. Filippi, M. Innocenti, A. Marchionni, W. Oberhauser, L. Wang, F. Vizza, Nanotechnology makes biomass electrolysis more energy efficient than water electrolysis, *Nat. Commun.* 5 (2014) 1–6, <https://doi.org/10.1038/ncomms5036>.
- [28] V. Bambagioni, M. Bevilacqua, C. Bianchini, J. Filippi, A. Marchionni, F. Vizza, L. Q. Wang, P.K. Shen, Ethylene glycol electrooxidation on smooth and nanostructured Pd electrodes in alkaline media, *Fuel Cells* (2010), <https://doi.org/10.1002/fuce.200900120>.
- [29] M. Bellini, J. Filippi, H.A. Miller, W. Oberhauser, F. Vizza, Q. He, H. Grützmacher, Hydrogen and chemicals from renewable alcohols by organometallic electroreforming, *ChemCatChem* 9 (2017) 746–750, <https://doi.org/10.1002/cctc.201601427>.
- [30] M. Bellini, M. Bevilacqua, M. Innocenti, A. Lavacchi, H.A. Miller, J. Filippi, A. Marchionni, W. Oberhauser, L. Wang, F. Vizza, Energy & chemicals from renewable resources by electrocatalysis, *J. Electrochem. Soc.* 161 (2014) D3032–D3043, <https://doi.org/10.1149/2.005407jes>.
- [31] J.B. Costa Santos, C. Vieira, R. Crisafulli, J.J. Linares, Promotional effect of auxiliary metals Bi on Pt, Pd, and Ag on Au, for glycerol electrolysis, *Int. J. Hydrog. Energy* 45 (2020) 25658–25671, <https://doi.org/10.1016/j.ijhydene.2019.11.225>.
- [32] R. Crisafulli, F.M. de Lino Amorim, S.M.L. de Oliveira Marconilio, W. Mendes Cunha, B.R. Brenda, J.A. Dias, J.J. Linares, Electrochemistry for biofuels waste valorization: vinasse as a reducing agent for Pt/C and its application to the electrolysis of glycerin and vinasse, *Electrochem. Commun.* 102 (2019) 25–30, <https://doi.org/10.1016/j.elecom.2019.03.012>.
- [33] J. De Paula, D. Nascimento, J.J. Linares, D.éborah Nascimento, J.J. Linares, Influence of the anolyte feed conditions on the performance of an alkaline glycerol electroreforming reactor, *J. Appl. Electrochem* 45 (2015) 689–700, <https://doi.org/10.1007/s10800-015-0848-6>.
- [34] H.J. Kim, Y. Kim, D. Lee, J.-R. Kim, H.-J. Chae, S.-Y. Jeong, B.-S. Kim, J. Lee, G. W. Huber, J. Byun, S. Kim, J. Han, Coproducing value-added chemicals and hydrogen with electrocatalytic glycerol oxidation technology: experimental and techno-economic investigations, *ACS Sustain. Chem. Eng.* 5 (2017) 6626–6634, <https://doi.org/10.1021/acssuschemeng.7b00868>.
- [35] M. Simões, S. Baranton, C. Coutanceau, Electrochemical valorisation of glycerol, *ChemSusChem* 5 (2012) 2106–2124, <https://doi.org/10.1002/cssc.201200335>.
- [36] S. Kongjao, S. Damronglerd, M. Hunsom, Electrochemical reforming of an acidic aqueous glycerol solution on Pt electrodes, *J. Appl. Electrochem.* 41 (2011) 215–222, <https://doi.org/10.1007/s10800-010-0226-3>.
- [37] J. González-Cobos, S. Baranton, C. Coutanceau, Development of bismuth-modified PtPd nanocatalysts for the electrochemical reforming of polyols into hydrogen and value-added chemicals, *ChemElectroChem* 3 (2016) 1694–1704, <https://doi.org/10.1002/celec.201600147>.
- [38] A.L. Yuvaraj, D. Santharaj, A systematic study on electrolytic production of hydrogen gas by using graphite as electrode, *Mater. Res.* 17 (2013) 83–87, <https://doi.org/10.1590/S1516-14392013005000153>.
- [39] M.S. Ardi, M.K. Aroua, N.A. Hashim, Progress, prospect and challenges in glycerol purification process: a review, *Renew. Sustain. Energy Rev.* 42 (2015) 1164–1173, <https://doi.org/10.1016/j.rser.2014.10.091>.
- [40] S. Maldonado, M. Rodrigo, P. Cañizares, G. Roa, C. Barrera, J. Ramirez, C. Sáez, On the degradation of 17- $\beta$  estradiol using boron doped diamond electrodes, *Processes* 8 (2020) 710, <https://doi.org/10.3390/pr8060710>.
- [41] J. De Paula, D. Nascimento, J.J. Linares Leon, Electrochemical reforming of glycerol in alkaline PBI-based PEM reactor for hydrogen production, *Chem. Eng. Trans.* 41 (2014) 205–210, <https://doi.org/10.3303/CET1441035>.
- [42] A.P. Nascimento, J.J. Linares, Performance of a direct glycerol fuel cell using KOH doped polybenzimidazole as electrolyte, *J. Braz. Chem. Soc.* 25 (2014) 509–516, <https://doi.org/10.5935/0103-5053.20140018>.
- [43] A. Regalado-Méndez, M.I. Bernabé Gutiérrez, P.N. Magaña Rivera, Y.S. Franco Molina, J. Cirilo González, E. Peralta-Reyes, C. Estrada Vázquez, J. Mentado-Morales, Producción de Biodiesel a Partir de Aceite de Cocina Reciclado por Destilación Reactiva Empleando Arena de Mar como Catalizador, in: X Encuentro Nac. La AMIDIQ, Academia Mexicana de Investigación y Docencia en Ingeniería Química A. C., San José del Cabo, 2018: p. TER 2–6.
- [44] A. Regalado-Méndez, N.I. Juárez-Bautista, J. Mentado-Morales, G.E. Leyte-Morales, M.E. Cordero, E. Peralta-Reyes, Estudio Paramétrico de la Producción de Biodiesel Empleando Aceite de Cocina Reciclado, Metanol y residuos Coralinos Como Catalizador, in: XL Encuentro Nac. La AMIDIQ, Academia Mexicana de Investigación y Docencia en Ingeniería Química A. C., Bahías de Huatulco, 2019: p. ENERGIA 11–15. [https://www.researchgate.net/publication/331566841\\_Estudio\\_Parametrico\\_de\\_la\\_Produccion\\_de\\_Biodiesel\\_Empleando\\_Aceite\\_de\\_Cocina\\_Reciclado\\_Metanol\\_y\\_residuos\\_Coralinos\\_Como\\_Catalizador](https://www.researchgate.net/publication/331566841_Estudio_Parametrico_de_la_Produccion_de_Biodiesel_Empleando_Aceite_de_Cocina_Reciclado_Metanol_y_residuos_Coralinos_Como_Catalizador).
- [45] A. Regalado-Méndez, D. Horta, M. Velázquez-Manzanares, L.G. Zárate, D.A. Vizarreta, E. Peralta-Reyes, Estudios de la Calidad de Biodiesel Sintetizado con Aceite de Cocina Reciclado, Metanol y Diferentes Catalizadores por Voltamperometría de Barrido Lineal y Espectroscopia de Impedancia, in: XL Encuentro Nac. La AMIDIQ, Academia Mexicana de Investigación y Docencia en Ingeniería Química A. C., Bahías de Huatulco, 2019: p. MATERIALES 27–31.
- [46] A. Regalado-Méndez, M. Ruiz, J.A. Hernández-Servín, R. Natividad, R. Romero, M. E. Cordero, C. Estrada-Vázquez, E. Peralta-Reyes, Electrochemical mineralization of ibuprofen on BDD electrodes in an electrochemical flow reactor: numerical optimization approach, *Processes* 8 (2020) 1666, <https://doi.org/10.3390/pr8121666>.
- [47] D.C. Montgomery, Design and analysis of experiments, 9th ed., John Wiley & Sons, Ltd, New Jersey, 2017.
- [48] ISO 14040:2006, Gestión ambiental. Análisis de ciclo de vida. Principios y marco de referencia, México, 2007.
- [49] ISO 14044, Environmental management — Life cycle assessment — Requirements and guidelines, 2006.
- [50] R. Zhou, M. Zhang, J. Li, W. Zhao, Optimization of preparation conditions for biochar derived from water hyacinth by using response surface methodology (RSM) and its application in Pb<sup>2+</sup> removal, *J. Environ. Chem. Eng.* 8 (2020), 104198, <https://doi.org/10.1016/j.jece.2020.104198>.
- [51] S. Dixit, V.L. Yadav, Optimization of polyethylene/polypropylene/alkali modified wheat straw composites for packaging application using RSM, *J. Clean. Prod.* 240 (2019), 118228, <https://doi.org/10.1016/j.jclepro.2019.118228>.
- [52] S.Q. Aziz, H.A. Aziz, M.S. Yusoff, M.J.K. Bashir, Landfill leachate treatment using powdered activated carbon augmented sequencing batch reactor (SBR) process: Optimization by response surface methodology, *J. Hazard. Mater.* 189 (2011) 404–413, <https://doi.org/10.1016/j.jhazmat.2011.02.052>.
- [53] S. Korde, S. Deshmukh, S. Tandekar, R. Jugade, Implementation of response surface methodology in physico-chemisorption of Indigo carmine dye using modified chitosan composite, *Carbohydr. Polym. Technol. Appl.* 2 (2021), 100081, <https://doi.org/10.1016/j.carpta.2021.100081>.
- [54] K. Barbusiński, S. Fajkis, B. Szelag, Optimization of soapstock splitting process to reduce the concentration of impurities in wastewater, *J. Clean. Prod.* 280 (2021), 124459, <https://doi.org/10.1016/j.jclepro.2020.124459>.
- [55] B. Petersen, P.A. Vanrolleghem, K. Gernaey, M. Henze, Evaluation of an ASM1 model calibration procedure on a municipal–industrial wastewater treatment plant, *J. Hydroinform.* 4 (2002) 15–38, <https://doi.org/10.1016/j.hydro.2002.0003>.
- [56] H.J. Kim, J. Lee, S.K. Green, G.W. Huber, W.B. Kim, Selective glycerol oxidation by electrocatalytic dehydrogenation, *ChemSusChem* 7 (2014) 1051–1056, <https://doi.org/10.1002/cssc.201301218>.
- [57] Y. Liu, R. Farauto, A. Lawal, Autothermal reforming of glycerol in a dual layer monolith catalyst, *Chem. Eng. Sci.* 89 (2013) 31–39, <https://doi.org/10.1016/j.ces.2012.11.030>.
- [58] M.M. Rahman, H<sub>2</sub> production from aqueous-phase reforming of glycerol over Cu–Ni bimetallic catalysts supported on carbon nanotubes, *Int. J. Hydrog. Energy* 40 (2015) 14833–14844, <https://doi.org/10.1016/j.ijhydene.2015.09.015>.
- [59] B. Dou, G.L. Rickett, V. Dupont, P.T. Williams, H. Chen, Y. Ding, M. Ghadiri, Steam reforming of crude glycerol with in situ CO<sub>2</sub> sorption, *Bioresour. Technol.* 101 (2010) 2436–2442, <https://doi.org/10.1016/j.biortech.2009.10.092>.
- [60] A. Shahedi, A.K. Darban, F. Taghipour, A. Jamshidi-Zanjani, A review on industrial wastewater treatment via electrocoagulation processes, *Curr. Opin. Electrochem* 22 (2020) 154–169, <https://doi.org/10.1016/j.coelec.2020.05.009>.
- [61] D. Ghosh, C.R. Medhi, M.K. Purkait, Techno-economic analysis for the electrocoagulation of fluoride-contaminated drinking water, *Toxicol. Environ. Chem.* 93 (2011) 424–437, <https://doi.org/10.1080/02772248.2010.542158>.
- [62] J. Vicker, D. Peterson, K. Randolph, Cost of Electrolytic Hydrogen Production with Existing Technology, Am. Department Energy United States Am., 2020, 5. <https://www.hydrogen.energy.gov/pdfs/20004-cost-electrolytic-hydrogen-production.pdf>.
- [63] G. Sasikumar, A. Muthumeenal, S.S. Pethaiah, N. Nachiappan, R. Balaji, Aqueous methanol electrolysis using proton conducting membrane for hydrogen production, *Int. J. Hydrog. Energy* 33 (2008) 5905–5910.
- [64] D.L. Stojić, M.P. Marčeta, S.P. Sovilj, S.S. Miljanić, Hydrogen generation from water electrolysis—possibilities of energy saving, *J. Power Sources* 118 (2003) 315–319, [https://doi.org/10.1016/S0378-7753\(03\)00077-6](https://doi.org/10.1016/S0378-7753(03)00077-6).
- [65] S. Shiva Kumar, V. Himabindu, Hydrogen production by PEM water electrolysis – a review, *Mater. Sci. Energy Technol.* 2 (2019) 442–454, <https://doi.org/10.1016/j.mset.2019.03.002>.
- [66] J. Chi, H. Yu, Water electrolysis based on renewable energy for hydrogen production, *Chin. J. Catal.* 39 (2018) 390–394, [https://doi.org/10.1016/S1872-2067\(17\)62949-8](https://doi.org/10.1016/S1872-2067(17)62949-8).
- [67] V. Bambagioni, M. Bevilacqua, C. Bianchini, J. Filippi, A. Lavacchi, A. Marchionni, F. Vizza, P.K. Shen, Self-sustainable production of hydrogen, chemicals, and energy from renewable alcohols by electrocatalysis, *Chem. Sustain. Energy Mater.* 3 (2010) 851–855, <https://doi.org/10.1002/cssc.201000103>.
- [68] M. Bellini, M.V. Pagliaro, A. Marchionni, J. Filippi, H.A. Miller, M. Bevilacqua, A. Lavacchi, W. Oberhauser, J. Mahmoudian, M. Innocenti, P. Fornasiero, F. Vizza, Hydrogen and chemicals from alcohols through electrochemical reforming by Pd-CeO<sub>2</sub>/C electrocatalyst, *Inorg. Chim. Acta* 518 (2021), 120245, <https://doi.org/10.1016/j.ica.2021.120245>.
- [69] K. Zakaria, R. Thimmappa, M. Mamlouk, K. Scott, Hydrogen generation by alcohol reforming in a tandem cell consisting of a coupled fuel cell and electrolyser, *Int. J. Hydrog. Energy* 45 (2020) 8107–8117, <https://doi.org/10.1016/j.ijhydene.2020.01.123>.
- [70] J. Brian, C. Whitney, M. Jennie, PEM Electrolysis H<sub>2</sub> A Production Case Study Documentation, Arlington, 2013. [https://www.hydrogen.energy.gov/pdfs/h2a\\_pem\\_electrolysis\\_case\\_study\\_documentation.pdf](https://www.hydrogen.energy.gov/pdfs/h2a_pem_electrolysis_case_study_documentation.pdf).

- [71] Q. Dai, A. Elgowainy, J. Kelly, J. Han, M. Wang, Life Cycle Analysis of Hydrogen Production from Non-Fossil Sources, 2016. <https://greet.es.anl.gov/publication-h2-nonfoss-2016>.
- [72] A. Al-Qahtani, B. Parkinson, K. Hellgardt, N. Shah, G. Guillen-Gosalbez, Uncovering the true cost of hydrogen production routes using life cycle monetisation, *Appl. Energy* 281 (2021), 115958, <https://doi.org/10.1016/j.apenergy.2020.115958>.
- [73] D. Melideo, R. Ortiz Cebolla, E. Weidner, Life Cycle Assessment of Hydrogen and Fuel Cell Technologies, Netherlands, 2019. [https://www.fch.europa.eu/sites/default/files/JRC116599\\_deliverable\\_b37\\_public\\_version%28ID 7366919%29.pdf](https://www.fch.europa.eu/sites/default/files/JRC116599_deliverable_b37_public_version%28ID%207366919%29.pdf).
- [74] Y.F. Khalil, Simulation-based environmental-impact assessment of glycerol-to-hydrogen conversion technologies, *Clean. Energy* 5 (2021) 387–402, <https://doi.org/10.1093/ce/zkab018>.
- [75] A. Susmozas, D. Iribarren, J. Dufour, Assessing the life-cycle performance of hydrogen production via biofuel reforming in Europe, *Resources* 4 (2015) 398–411, <https://doi.org/10.3390/resources4020398>.
- [76] O. Siddiqui, I. Dincer, A well to pump life cycle environmental impact assessment of some hydrogen production routes, *Int. J. Hydrog. Energy* 44 (2019) 5773–5786, <https://doi.org/10.1016/j.ijhydene.2019.01.118>.